IEEE Photonics Journal
An IEEE Photonics Society Publication

Open Access

Drop-Casted Self-Assembled Topological Insulator Membrane as an Effective Saturable Absorber for Ultrafast Laser Photonics

Volume 7, Number 2, April 2015

Qingkai Wang
Yu Chen
Guobao Jiang
Lili Miao
Chujun Zhao
Xiquan Fu
Shuangchun Wen
Han Zhang

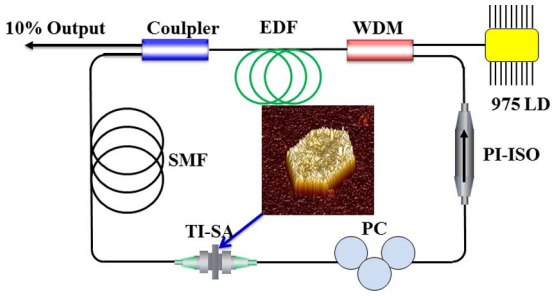

DOI: 10.1109/JPHOT.2015.2406754
1943-0655

Drop-Casted Self-Assembled Topological Insulator Membrane as an Effective Saturable Absorber for Ultrafast Laser Photonics

Qingkai Wang,[1,4] Yu Chen,[2] Guobao Jiang,[3] Lili Miao,[3] Chujun Zhao,[2] Xiquan Fu,[1] Shuangchun Wen,[3] and Han Zhang[3]

[1]Key Laboratory for Micro-/Nano-Optoelectronic Devices of Ministry of Education, College of Computer Science and Electronic Engineering, Hunan University, Changsha 410082, China
[2]SZU-NUS Collaborative Innovation Center for Optoelectronic Science and Technology, Key Laboratory of Optoelectronic Devices and Systems of Ministry of Education and Guangdong Province, College of Optoelectronic Engineering, Shenzhen University, Shenzhen 518060, China
[3]Key Laboratory for Micro-/Nano-Optoelectronic Devices of Ministry of Education, College of Physics and Microelectronic Science, Hunan University, Changsha 410082, China
[4]College of Science, Jiujiang University, Jiujiang 332005, China

DOI: 10.1109/JPHOT.2015.2406754

Manuscript received December 16, 2014; revised February 5, 2015; accepted February 19, 2015. Date of publication March 2, 2015; date of current version March 5, 2015. This work was supported in part by the Ministry of Education under Grant NCET 11-0135; by the National Natural Science Fund under Grant 61222505, Grant 61435010, and Grant 61475102; and by Hunan Provincial Natural Science Foundation of China under Grant 13JJ1012. Q. Wang and Y. Chen contributed equally to this work. Corresponding author: H. Zhang (e-mail: hzhang@szu.edu.cn).

Abstract: Through employing a cost-effective solvothermal method, ultrathin topological insulator (TI) bismuth telluride (Bi_2Te_3) nanosheets with uniform hexagonal nanostructures had been synthesized. Thanks to the uniformity of few-layer TI dispersion, we are able to adopt the drop-casting approach in order to directly transfer few-layer TI and, therefore, form a self-assembled uniform volatile TI membrane that is suitably deposited onto the end facet of an optical fiber as an effective optical saturable absorber. Its saturable absorption parameters could be deliberately tailored by thinning its thickness by mechanical exfoliation. The incorporation of the as-fabricated saturable absorber inside the fiber laser cavity allows for the operation of either a microsecond or a femtosecond pulse because different saturable absorption parameters can decide whether the fiber laser operates in the mode-locking or Q-switching state. Our work provides a convenient way of fabricating a high-quality TI membrane-based saturable absorber with promising applications for laser operation.

Index Terms: Topological insulator, mode-locking, Q-switching, self-assembled.

1. Introduction

Topological insulators (TIs) are typical functional nanostructures that have a bulk band gap like an ordinary insulator but a protected conducting state on their edge or surface [1], [2]. These unique properties originate from the combined effects of spin-orbit interactions and time-reversal symmetry [3]. The joint action of the small bulky band-gap and the gap-less surface state render

TIs with ultra-broadband nonlinear optical response ranging from the visible to the microwave frequency [4]. The first demonstration of the saturable absorption in TI nano-materials and related applications for ultra-fast laser photonics [5] had led to a rising wave of the exploration of photonics with TI. Particularly, several different research groups have taken the advantages of the broadband saturable absorption in TI for the broadband pulsed laser operation at various wavelengths, from infrared to mid-infrared [6]–[16]. Therefore TI materials have been considered as one of the few viable substitute materials for traditional saturable absorber (SA), such as semiconductor saturable absorber mirrors (SESAM) [17], carbon nanotube (CNT) [18], [19], and graphene [20]–[31]. Different from those conventional saturable absorber materials, TI possesses one intrinsic advantage that its optical property, in association with its surface mass-less Dirac electron states, is more robust against external perturbations. This is because its metallic surface state, which is a natural result of the strong spin-orbital coupling, is very stable and able to withstand unexpected impurities or defects [32]. However, up to now, lack of high quality materials and effective transfer technology may delimit further investigations. In this contribution, we aimed at partially solving these problems, and therefore employ a well-improved fabrication approach in order to produce small particle size TI-based nano-materials followed with a new transfer technology, together of which led to the successful demonstration of a cost-effective and high-performance TI-based optical device. Several different methods had been proposed to synthesize few-layer TIs, including peeling-off from the bulk materials by an atomic force microscope tip [33], mechanical exfoliation [34], molecular beam epitaxial growth [35], electrochemical deposition [36], hydrothermal intercalation [37], and solvothermal synthesis [38]–[40]. Among those methods, the solvothermal process is considered as a convenient one capable of mass-producing nanostructured TI-based materials with small particle size, desired structures and morphologies. More importantly, volume production and small particle size is an important issue that we must take into consideration in order to fulfill the requirements of the optical applications of few-layer TIs. Herein, we used a facile solvothermal method to synthesize Bi_2Te_3 hexagonal nanosheets, allowing for the production of large scale and high quality samples that well fit for the optical investigation. On the other hand, the process of transferring TI onto the target substrate is also another key technology for fabricating TI-based optical devices. There had emerged various transferring methods, including polymer composite membrane [9], [10] with fiber ferrules, optical deposition [41], direct deposition of a bulk material onto side-polished fibers [6], and drop-casting [4], [45]. However, those as-mentioned methods possess some intrinsic disadvantages. For example, the incorporation of polymer composite membrane could introduce unwanted organics and impurities, resulting in additional scattering loss. Also, polymer membranes may possess low damage threshold that will reduce the damage threshold of the whole TI-optical device, further limiting its potential applications towards high power regime. Optical deposition needs extra light source which complicates the transfer process, and furthermore its success rate is quite low, making this approach relatively cost-ineffective. Drop-casting may be the simplest transfer method. However, according to some previous contributions [4], owing to the heterogeneity of TI dispersion, the TI-based film forming on the substrate surface is asymmetric so that the optical device cannot be fabricated with high-efficiency.

In this paper, we proposed a face-to-face drop-casted transfer method to fabricate TI-based saturable absorber device. Hexagonal uniform-sized and ultra-thin Bi_2Te_3 nanosheets were prepared through facile solvothermal method and well dispersed into ethanol solution. Then, by drop casting Bi_2Te_3 dispersion directly onto the fiber ferrule, the nanosheets turn into layers of a uniform volatile film on the fiber ferrule after gradual volatilization of ethanol solution. By placing the as-formed saturable absorber into the fiber laser cavity, stable Q-switching with large single pulse energy up to 200 nJ had be observed. In this case, the Bi_2Te_3 volatile film is relatively thick. In order to achieve the mode-locking operation, we peel off the Bi_2Te_3 volatile film into thinner one by scotch tape in order that the saturable absorption parameters are modified. Under this case, femtosecond mode- locking with pulse duration of 448 fs can be obtained. This shows the robustness and feasibility of the TI-saturable absorber that could be used for either micro-second and femto-second laser operation.

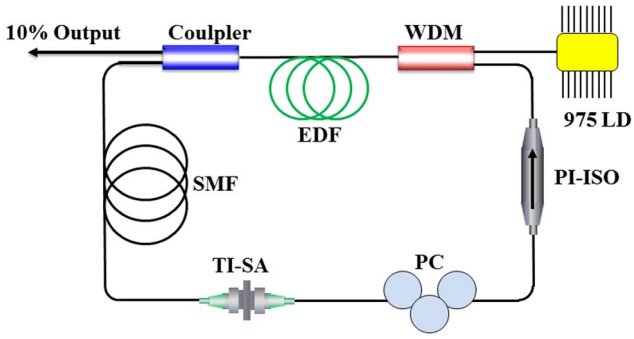

Fig. 1. Experimental setup of fiber laser.

2. Experimental Setup

2.1. Synthesis of Bi_2Te_3 Film

Currently, in a typical synthesis, a stoichiometric ratio of bismuth chloride (BiCl3), and sodium selenide (Na2TeO3) were dissolved in ethylene glycol with vigorous stirring. Then the mixture was transferred into a stainless steel autoclave with Teflon lining up to 80% of the capacity. The autoclave was heated at 200 °C in an electric oven and then cooled down to room temperature naturally. The gray powders were collected by filtering, washed with distilled water and ethanol, and finally dried at 60 °C in vacuum. The as-grown and washed powders were dispersed in an ethanol solution. Then, we drop casted the Bi_2Te_3 dispersion directly onto the fiber ferrule. Once the ethanol was volatilized, the nanosheets would form a uniform volatile film on the fiber ferrule contributed to the high uniformity of the TI dispersion.

2.2. Fiber Laser

The schematic diagram of the TI-based all-fiber laser is shown in Fig. 1. The whole cavity consists of erbium-doped fiber (EDF), standard single mode fiber (SMF), wavelength division multiplexer (WDM), polarization independent isolator (PII-ISO), output coupler, polarization controller (PC), and TI-SA. WDM is used as the pump and feedback coupling, and the 10% port of a coupler as output. EDF (LIEKKI Er 80-8/125) is used as gain medium with 0.95 meter, the rest of the cavity is all SMF with total length of 38 meter. The unidirectional operation of the ring cavity is ensured by PII-ISO. PC is used to optimize the performance of the fiber laser. The packed TI-SA sandwiched by fiber ferrules acts a SA.

3. Experimental Results

3.1. Structure and Morphology of Bi_2Te_3 Nanosheets

The morphology and size of the as-prepared Bi_2Te_3 samples were characterized by field-emission scanning electron microscopy (FESEM, JSM-6700F) and transmission electron microscopy (TEM, JEOL 3010). The lower magnification FESEM image [see Fig. 2(a)] reveals that a large number of sheet-like structures are randomly dispersed on the substrate. The obtained products are predominantly hexagonal-based sheets of uniform size and well-defined shape. A higher magnification FESEM image [see Fig. 2(b)] shows that the edge length of sheets is in the range of 400–600 nm, and that their thickness is about 15 nm. TEM provides further insight into the microstructural details of the Bi_2Te_3 nanostructures. Fig. 2(c) is a typical TEM image of a single nanosheet, which clearly demonstrates the nanosheet has perfect hexagonal morphology. To further confirm the thickness and the width of as-prepared Bi_2Te_3 nanosheets, the AFM topography images (Multimode 8 system) of Bi_2Te_3 nanosheets are investigated. As shown in

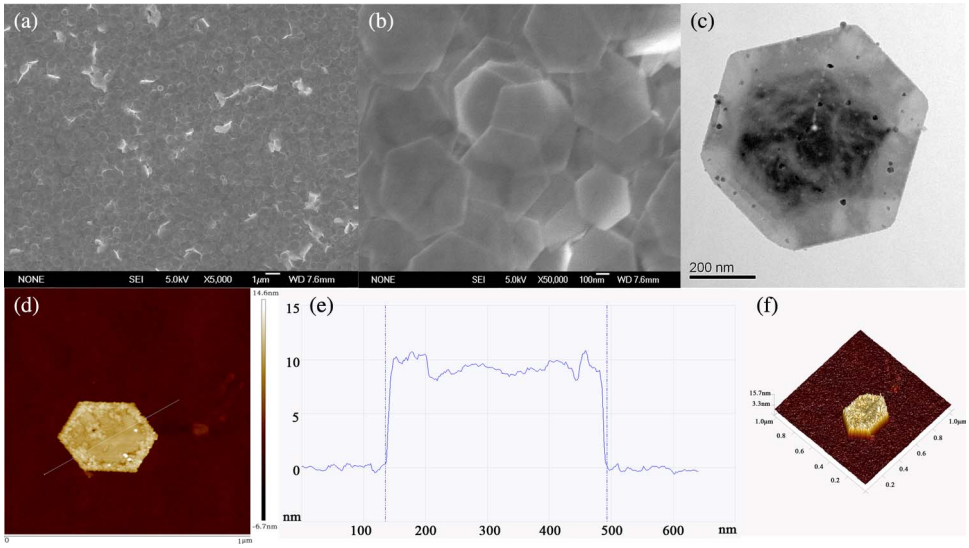

Fig. 2. (a) Low-magnification FESEM image of Bi_2Te_3 nanosheets. (b) High-magnification FESEM image of Bi_2Te_3 nanosheets. (c) TEM image of a single perfect hexagonal nanosheet. (d) Topographic AFM images of the Bi_2Te_3 nanosheet. (e) Corresponding height profiles. (f) Corresponding 3-D images.

Fig. 2, the Bi_2Te_3 nanosheet has flat surface with a uniform thickness about 15 nm across the lateral dimensions. The height profiles corresponding to the line-cut in Fig. 2(e) is shown in Fig. 2(e). The two dotted lines in Fig. 2(e) correspond to the two blue points of the line-cut in Fig. 2(d). The width of the Bi_2Te_3 nanosheet is about 400 nm, which is represented by the distance between the two dotted lines.

The X-ray diffraction (XRD, D8-Advanee X-ray diffractometer with a Cu-Kα radiation) pattern of the as-prepared products is shown in Fig. 3(a). All the diffraction peaks can be indexed to rhombohedral Bi_2Te_3 (space group: $R\bar{3}$m) with lattice constants a = b = 0.438 nm, c = 3.05 nm, which are consistent with the literature values (JCPDS No. 15-0863). This result indicates that Bi_2Te_3 products obtained via our synthetic method consist of a pure phase. Through performing the Raman characterization on the as-prepared Bi_2Te_3 nanosheets by Raman Labram-010 system, we have measured the corresponding Raman spectra, as shown in Fig. 3(b). The spectrum contains four main peaks which correspond to A^1_{1g}, E^2_g, A_{1u}, and A^2_{1g} respectively. The Raman spectrum of bulk polycrystalline Bi_2Te_3 exhibits three signature optical phonon modes, including A^1_{1g}, E^2_g, and A^2_{1g}. The as-prepared Bi_2Te_3 nanosheets exhibit an extra infrared active phonon mode, A_{1u} mode, which is not found in the bulk phase. It is possible that the ultrathin layered structure allows for the symmetry breakup the centro-symmetric nature of Bi_2Te_3 for the observation of A_{1u} mode. Based on the above characterization results, we can conclude that our sample possesses high quality in terms of large size and uniformity. We also tested the long term stabilization of the Bi_2Te_3 dispersion and found that after 2 months, the Bi_2Te_3 nanosheets had not ever been precipitated and still uniformly distributed in solution, mostly attribute to the small size of Bi_2Te_3 nanosheets. The admirable uniformity enables the Bi_2Te_3 nanosheets to form a uniform volatile TI membrane when the alcohol volatilize completely, improving the mission success rate and effective percentage of the SA device preparation.

3.2. Passively Q-Switched Fiber Lasers

The as-prepared Bi_2Te_3 dispersion can be directly dropped casting onto the end-facet of a standard FC/PC fiber ferrule. After the volatilization of ethanol solution, the Bi_2Te_3 nanosheets turned into a thicker film on the fiber ferrule. By connecting another FC/PC fiber ferrule, the

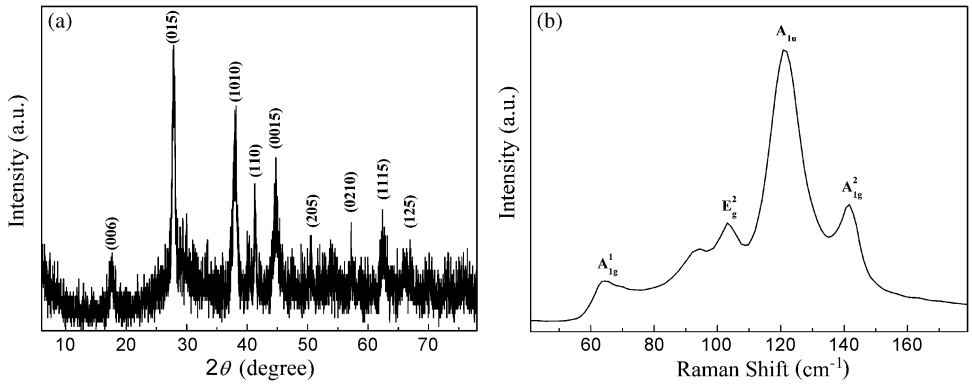

Fig. 3. (a) XRD patterns of the as-prepared Bi_2Te_3. (b) Raman spectra of Bi_2Te_3 at 632 nm laser excitation.

TI-SA all-fiber device was successfully achieved. After then, the TI-SA device was spliced into the continuous wave (CW) Er-doped fiber laser, the Q-switching pulse emission could be obtained. The Q-switching operation starts at a pump power of 43 mW with lasing threshold of 30 mW. The relatively high self-starting threshold for Q-switched operation is attributed to the high saturable intensity of TIs. Fig. 4 describes the characteristics of typical Q-switched pulses emitted from the fiber laser at a pump power of 105.7 mW. Based on a 500 MHz oscilloscope (Tektronix TDS3054B) combined with a 5 GHz photo-detector (Thorlabs SIR5), the output pulse train has been characterized in Fig. 4(a). It has a pulse repetition rate of 6.239 kHz, corresponding to a pulse interval of 163.3 μs. As can be seen, it has a uniform pulse peak intensity without any obvious pulse jitter, which revealing the high stability of Q-switching operation. Fig. 4(b) is the corresponding spectrum measured by an optical spectrum analyzer (Ando AQ-6317B) with a resolution of 0.015 nm. The central wavelength is measured to be 1567.1 nm. The internal fine structure of the optical pulse is also investigated at a small time scale with more sampling points, as shown in Fig. 4(c). It can be seen that the pulse duration is inferred to be about 18.4 μs, and the absence of intensity modulation suggests that the Q-switching instability had been effectively suppressed.

At a fixed cavity polarization setting, through gradually increasing the pump power, the representative Q-switching could be summarized in Fig. 5. The pulse interval could gradually decease with the increasing of the pump power. This suggests that the corresponding cavity repetition rate could increase. More importantly, during this evolution process, the pulse train remains a uniform intensity distribution, which shows relatively high stability of the passive Q-switching operation. Once the pump power exceeds 201.7 mW, strong amplitude fluctuation of the Q-switching pulse starts to emerge and the Q-switching state become unstable, and eventually it could finally disappear, which is probably attributed to the optical bleaching of TI-SA under high power illumination.

Besides, we investigate the variation of pulse durations, pulse repetition rates, output average power, and single pulse energy as the pump power increases, as shown in Fig. 6. Fig. 6(a) shows the relation between output power, pulse energy and pump power. From which, the output average power increases gradually from 0.05 mW to 3.54 mW, and the maximum pulse energy can reach up to 278.8 nJ. As can be seen in Fig. 6(b), pulse repetition rate can be widely changed from 3.312 kHz to 12.74 kHz almost linearly, but the pulse duration non-linearly decreased from 44 μs to 12.74 μs.

3.3. Passively Mode-Locked Femtosecond Fiber Lasers

After achieving the Q-switching fiber laser, we took out the TI-SA from the fiber optical flange. Through repeatedly pressing slightly the scotch tape on the surface of the TI material

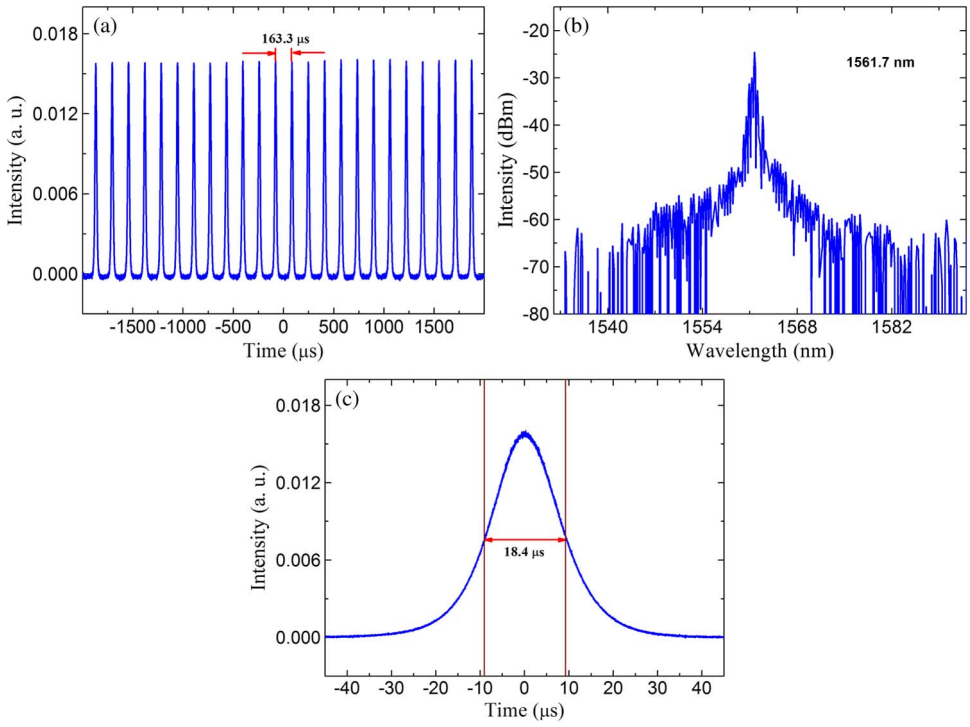

Fig. 4. Typical Q-switching output at a pump power of 105.7 mW. (a) Pulse train. (b) Corresponding output optical spectrum. (c) Single pulse profile.

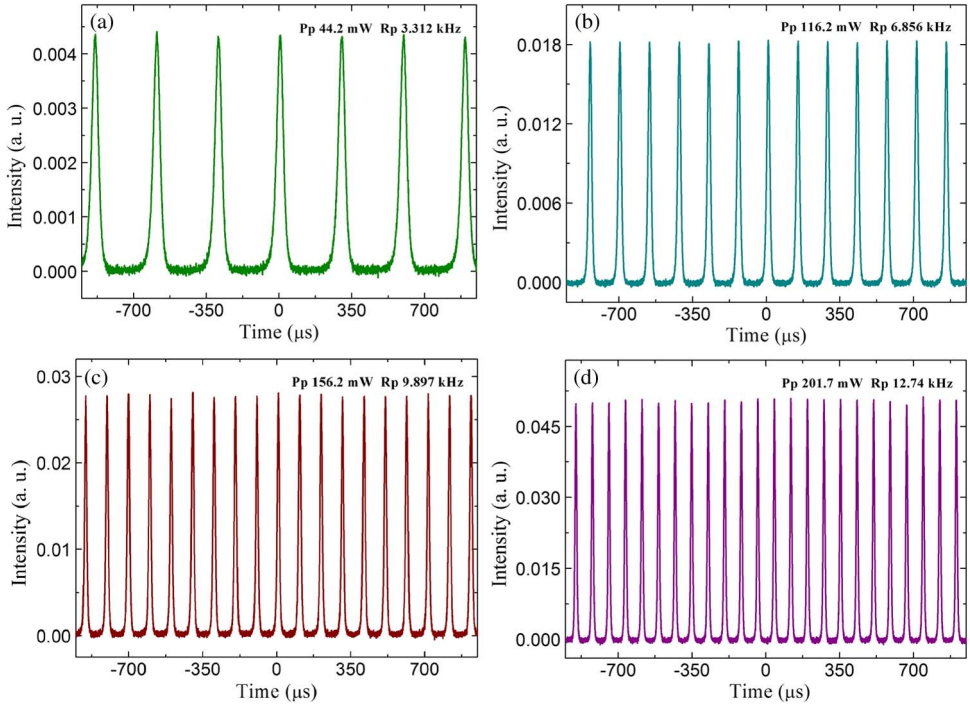

Fig. 5. Various pulse trains of the Q-switched pulses under different pump powers.

that is attached to the fiber end-facet, the relatively thick TI nanosheets could be moderately peeled into a thinner one, which could correspondingly alter its nonlinear optical property. In the following, we measured the nonlinear absorption characteristics of TI-SAs before and after

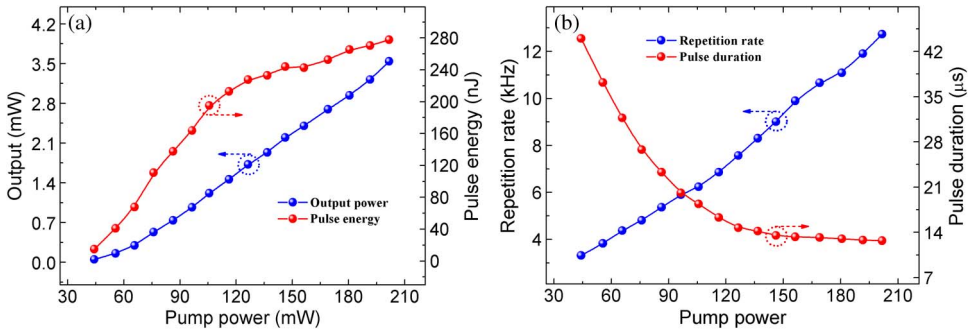

Fig. 6. Output average power and pulse energy. (b) Pulse repetition rate and duration with respect to different pump powers.

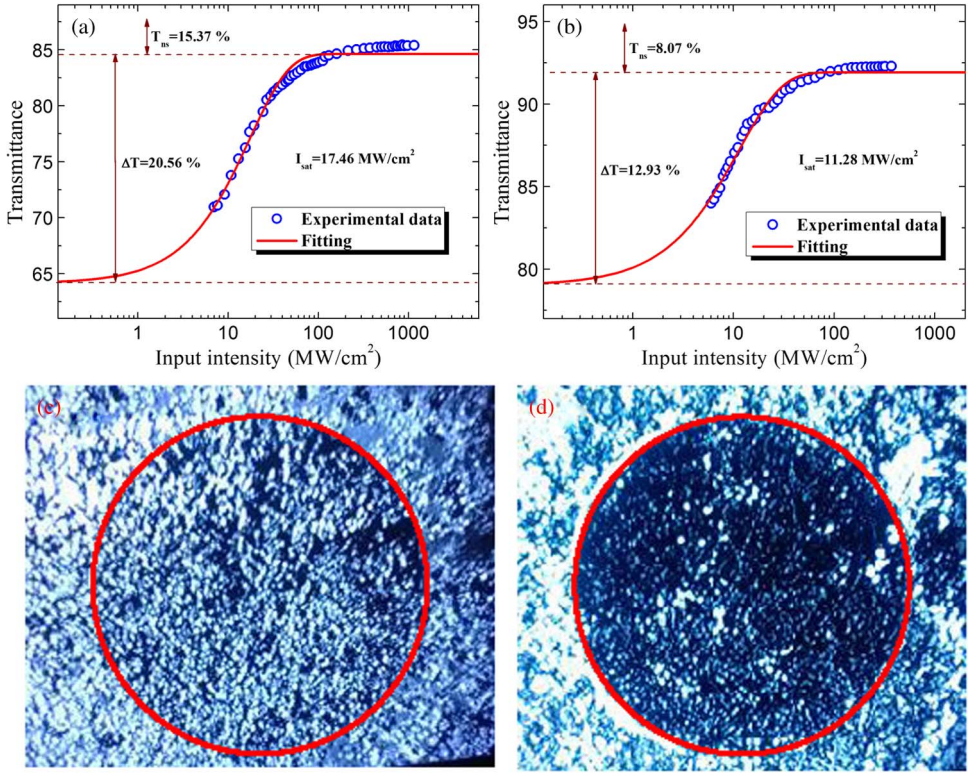

Fig. 7. Measured saturable absorption data and its corresponding fitting curves of TI-SAs before (a) and after (b) mechanical peeling; photograph of fiber end surface before (c) and after (d) the mechanical peeling process.

the mechanical peeling-off, as shown in Fig. 7. Upon fitting the measured experimental data with the widely used formula $T(I) = 1 - \Delta T * \exp(-I/I_{sat}) - T_{ns}$ ($T(I)$ is the transmission, ΔT is the modulation depth, I is the input intensity, I_{sat} is the saturation power intensity, and T_{ns} is the non-saturable absorbance), one can infer the corresponding saturable absorption parameters. As shown in Table 1, the modulation depth, saturation intensity and non-saturable absorbance are 20.56%, 17.46 MW/cm^2, and 15.37% before peeling, as showing in Fig. 7(a). After peeling [see Fig. 7(b)], then those parameters are changed to be 12.93%, 11.28 MW/cm^2, 8.07%. Obviously, the modulation depth and saturation intensity had been decreased

TABLE 1

The nonlinear absorption parameters (saturating intensity, modulation depth, non-saturable absorbance) before and after mechanical peeling

Case	Before	After
Saturating intensity (MW/cm^2)	17.46	11.28
Modulation depth	20.56 %	12.93 %
Non-saturable absorbance	15.37 %	8.07 %

through mechanical exfoliation, indicating that the TI-SA now becomes thinner. Also, we measured the insertion loss of these SA devices with 1550 nm CW. The insertion loss of TI-SA devices are 1.9 dB and 1.02 dB before and after mechanical peeling respectively. From the photography of fiber end surface before [see Fig. 7(c)] and after [see Fig. 7(d)] the mechanical peeling-off, we could clearly see that the thickness of the SA after mechanical peeling decreased obviously (the red circle is the fiber cladding with diameter of 125 μm).

After mechanical peeling the TI sample, when we insert the thinner one into laser cavity, stable mode-locking can be obtained immediately with the same cavity length. To obtain femtosecond pulse output and further verify the effectiveness of TI-SA, we have shorten the laser cavity. Inside the cavity, an extra piece of SMF has been removed so that the fiber ring laser cavity is shortened to 11.65 m. Self-starting stable mode-locking can be obtained at a pump power of 67 mW, which is relatively high because of the high saturation intensity of the saturable absorber [5], [10]. Fig. 8 summarizes the typical mode-locking operation of the fiber laser at a pump power of 101 mW. Fig. 8(a) shows the output pulse train recorded by an oscilloscope with a time span of 1 microsecond. The optical pulses are equidistantly distributed with uniform peak-intensity and a pulse repetition rate of 17.76 MHz, corresponding to a fundamental cavity frequency determined by the cavity length. This indicates that the pulse train operates in a stable mode-locking state. The insert shows the pulse train at a large scale of 20 μs, from which the amplitude modulation is not observed. The current output power is 3.6 mW, suggesting that per-pulse energy is about 0.203 nJ. Once the pump power exceeds 150 mW, pulse train becomes unstable and finally evolves into the multi-pulse state. To confirm whether the mode-locking state operates in soliton regime, the corresponding optical spectrum had been measured in Fig. 8(b). It has a central wavelength of 1565.9 nm with a full width at half maximum (FWHM) bandwidth of 5.75 nm. The appearance of symmetric Kelly sidebands verifies that the output pulses had been shaped into conventional solitons, which is a natural balance between the intra-cavity dispersion and optical nonlinearity [44]. We also study the pulse profile with an auto-correlation function analyzer, as shown in Fig. 8(c). The trace is closer to the hyperbolic secant profile. Through fitting with sech^2 function, the real pulse width is inferred to be 448 fs. Thus, the time-bandwidth product (TBP) is calculated as 0.316, which is pretty close to the value of transmission limiting and indicates that the pulse is almost non-chirped. Furthermore, there is no pedestal or other pulse in the auto-correlation trace confirming the high quality of mode locking and single pulse output state. Fig. 8(d) is the homologous radio frequency (RF) spectrum with span of 5 MHz, resolution bandwidth (RBW) of 30 Hz, video bandwidth (VBW) of 30 Hz. The central frequency is 17.76 MHz agreed with the measuring results of time domain. The signal-to-noise ratio (SNR) is up to 76 dB. The insert shows the RF spectrum within a frequency span of 1 GHz, from which, there is no extra frequency component except the fundamental and harmonic frequencies, which verifies the low-amplitude fluctuations, single pulse state and the high stability of output pulse train.

To investigate the long-term stability of the mode-locked laser pulse, we also record the output optical spectra every hour over 8 hours with fixed laser conditions using the auto recording function of optical spectrum analyzer, as shown in Fig. 9. During this process, neither central wavelength drifting nor new wavelength components had been observed.

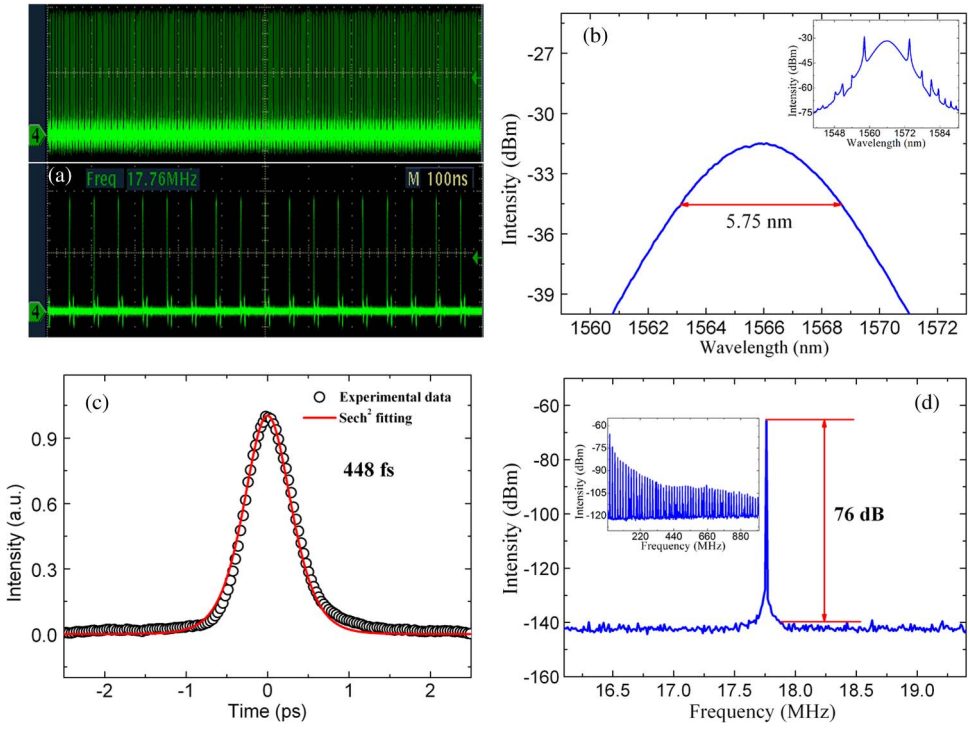

Fig. 8. Typical mode-locking output. (a) Output pulse train. (b) Corresponding spectrum. (c) Measured autocorrelation trace and its fitting curve. (d) RF spectrum. Inset: RF spectrum in 1 GHz span.

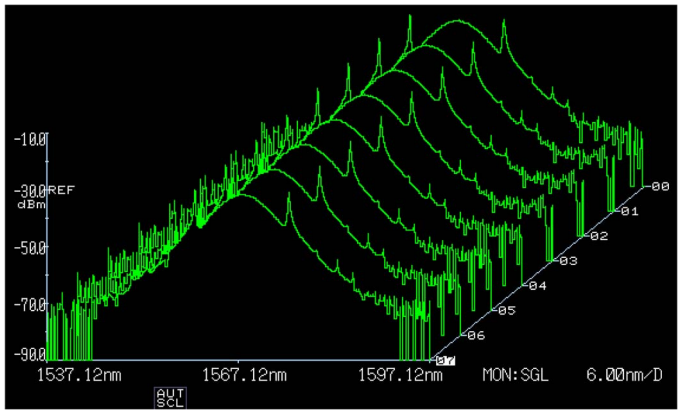

Fig. 9. Long-term spectra evolution measured at a 1 hour intervals over 8 hours.

4. Discussions

To the best of our knowledge, whether the fiber laser operates in Q-switching or mode locking state depends on the saturation parameters of the SA and the cavity configuration, especially the selection of SA. To get stable CW mode-locking without Q-switching instabilities, the following criterion should be fulfilled [42], [43]:

$$E_p^2 > E_{sat,G} E_{sat,SA} \Delta R$$

where, E_P is the single pulse energy in the cavity, $E_{sat,G}$ is the saturation energy of the gain, $E_{sat,SA}$ is the saturation energy of the SA, and ΔR is the modulation depth of the SA.

$E_{sat,G}E_{sat,SA}\Delta R$ is the minimum intra-cavity pulse energy required for obtaining stable CW mode locking. If $E_p^2 > E_{sat,G}E_{sat,SA}\Delta R$, it will allow for the operation of CW mode-locking. Otherwise, Q-switched mode- locking or Q-switching operation will emerge. Obviously, $E_{sat,G}$ is a fixed parameter in the same fiber laser cavity and the only factor that can change the value of $E_{sat,G}E_{sat,SA}\Delta R$ will be the saturable absorber component. Before peeling, the modulation depth and saturation energy of the TI-SA is relatively high causing that the value of $E_{sat,G}E_{sat,SA}\Delta R$ is relatively large. In this case, the Q-switching operation is more easily to be achieved. After peeling treatment, the layers number of TI-SA has been decreased and the modulation depth ΔR and saturation energy $E_{sat,SA}$ become smaller obviously, which makes the value of $E_{sat,G}E_{sat,SA}\Delta R$ be much smaller in a similar cavity setup. In this case, the E_P will be much easier to exceed $E_{sat,G}E_{sat,SA}\Delta R$ and the CW mode-locking state can be readily obtained. It suggests that mechanical exfoliation technique may usefully be applied to tailor the saturable absorber performance in association with the corresponding specific laser operation state, which may provide a new insight for the development of laser technology.

5. Conclusion

We have demonstrated a simple transfer method to fabricate the topological insulator (TI) based all-fibered SA device and demonstrated its ability for the generation of microsecond pulse and femtosecond pulse in a fiber laser cavity. By deliberately controlling the thickness of the TI sample, which corresponds to change the saturable absorption parameters of the as-fabricated SA device, two different types of pulsed laser operation states had been successfully demonstrated: One is high quality Q-switching with large per-pulse energy of 278.8 nJ if the SA film is thicker, and the other is femo-second mode-locking (with pulse duration down to 448 fs) if we peel off the Bi_2Te_3 film on the fiber ending using scotch tape and shorten the cavity length. Our work provides a simple and effective method to manufacture fibered SA device for researchers. More importantly, this work might benefit the development of high performance atomically thin semiconducting transition metal dichalcogenides, $MX_2(M = Mo, W; X = S, Se, Te)$ based optoelectronic devices that could find applications in ultra-fast laser photonics.

References

[1] M. Z. Hasan and C. L. Kane, "Colloquium: Topological insulators," *Rev. Mod. Phys.*, vol. 82, no. 4, pp. 3045–3067, Nov. 2010.

[2] G. Wang *et al.*, "Atomically smooth ultrathin films of topological insulator Sb_2Te_3," *Nano Res.*, vol. 3, no. 12, pp. 874–880, Dec. 2010.

[3] H. Zhang *et al.*, "Topological insulators in Bi_2Se_3, Bi_2Te_3 and Sb_2Te_3 with a single Dirac cone on the surface," *Nature Phys.*, vol. 5, no. 6, pp. 438–442, May 2009.

[4] X. Zhang, J. Wang, and S. C. Zhang, "Topological insulators for high-performance terahertz to infrared applications," *Phys. Rev. B*, vol. 82, no. 24, Dec. 2010, Art. ID. 245107.

[5] C. Zhao *et al.*, "Ultra-short pulse generation by a topological insulator based saturable absorber," *Appl. Phys. Lett.*, vol. 101, no. 21, Nov. 2012, Art. ID. 211106.

[6] Z. Luo *et al.*, "1.06 μm Q-switched ytterbium-doped fiber laser using few-layer topological insulator Bi_2Se_3 as a saturable absorber," *Opt. Express*, vol. 21, no. 24, pp. 29 516–29 522, Dec. 2013.

[7] M. Jung *et al.*, "A femtosecond pulse fiber laser at 1935 nm using a bulk-structured Bi_2Te_3 topological insulator," *Opt. Express*, vol. 22, no. 7, pp. 7865–7874, Apr. 2014.

[8] H. Yu *et al.*, "Topological insulator as an optical modulator for pulsed solid-state lasers," *Laser Photon. Rev.*, vol. 7, no. 6, pp. L77–L83, Nov. 2013.

[9] J. Sotor *et al.*, "Mode-locking in Er-doped fiber laser based on mechanically exfoliated Sb_2Te_3 saturable absorber," *Opt. Mater. Express*, vol. 4, no. 1, pp. 1–6, Jan. 2014.

[10] Y. Lin *et al.*, "Soliton compression of the erbium-doped fiber laser weakly started mode-locking by nanoscale p-type Bi_2Te_3 topological insulator particles," *Laser Phys. Lett.*, vol. 11, no. 5, May 2014, Art. ID. 055107.

[11] H. Liu *et al.*, "Femtosecond pulse generation from a topological insulator mode-locked fiber laser," *Opt. Express*, vol. 22, no. 6, pp. 6868–6873, Mar. 2014.

[12] P. Tang *et al.*, "Topological insulator: Bi_2Te_3 saturable absorber for the passive Q-switching operation of an in-band pumped 1645-nm Er:YAG ceramic laser," *IEEE Photon. J.*, vol. 5, no. 2, Apr. 2013, Art. ID. 1500707.

[13] J. Sotor, G. Sobon, W. Macherzynski, and K. Abramski, "Harmonically mode-locked Er-doped fiber laser based on a Sb_2Te_3 topological insulator saturable absorber," *Laser Phys. Lett.*, vol. 11, no. 5, May 2014, Art. ID. 055102.

[14] J. Lee, J. Koo, Y. Jhon, and J. Lee, "A femtosecond pulse erbium fiber laser incorporating a saturable absorber based on bulk-structured Bi_2Te_3 topological insulator," *Opt. Express*, vol. 22, no. 5, pp. 6165–6173, Mar. 2014.
[15] Z. Luo *et al.*, "2 GHz passively harmonic mode-locked fiber laser by a microfiber-based topological insulator saturable absorber," *Opt. Lett.*, vol. 38, no. 24, pp. 5212–5215, Dec. 2013.
[16] Z. Yu *et al.*, "High-repetition-rate Q-switched fiber laser with high quality topological insulator Bi_2Se_3 film," *Opt. Express*, vol. 22, no. 10, pp. 11 508–11 515, Dec. 2014.
[17] R. Paschotta *et al.*, "Passively Q-switched 0.1-mJ fiber laser system at 1.53 μm," *Opt. Lett.*, vol. 24, no. 6, pp. 388–390, Mar. 1999.
[18] Z. Sun *et al.*, "Ultrafast stretched-pulse fiber laser mode-locked by carbon nanotubes," *Nano Res.*, vol. 3, no. 6, pp. 404–411, Jun. 2010.
[19] A. Tausenev *et al.*, "177 fs erbium-doped fiber laser mode locked with a cellulose polymer film containing single-wall carbon nanotubes," *Appl. Phys. Lett.*, vol. 92, no. 17, Jun. 2008, Art. ID. 171113.
[20] Q. Bao *et al.*, "Monolayer graphene as a saturable absorber in a mode-locked laser," *Nano Res.*, vol. 4, no. 3, pp. 297–307, Mar. 2011.
[21] Z. Sun *et al.*, "Graphene mode-locked ultrafast laser," *ACS Nano*, vol. 4, no. 2, pp. 803–810, Jan. 2010.
[22] Q. Bao *et al.*, "Atomic-layer graphene as a saturable absorber for ultrafast pulsed lasers," *Adv. Funct. Mater.*, vol. 19, no. 19, pp. 3077–3083, Oct. 2009.
[23] Y. Song, S. Jang, W. Han, and M. Bae, "Graphene mode-lockers for fiber lasers functioned with evanescent field interaction," *Appl. Phys. Lett.*, vol. 96, no. 5, Feb. 2010, Art. ID. 051122.
[24] A. Martinez, K. Fuse, and S. Yamashita, "Mechanical exfoliation of graphene for the passive mode-locking of fiber lasers," *Appl. Phys. Lett.*, vol. 99, no. 12, Sep. 2011, Art. ID. 121107.
[25] J. Liu, S. Wu, Q. Yang, and P. Wang, "Stable nanosecond pulse generation from a graphene-based passively Q-switched Yb-doped fiber laser," *Opt. Lett.*, vol. 36, no. 20, pp. 4008–4010, Oct. 2011.
[26] M. Zhang *et al.*, "Tm-doped fiber laser mode-locked by graphene-polymer composite," *Opt. Express*, vol. 20, no. 22, pp. 25 077–25 084, Oct. 2012.
[27] J. Sotor *et al.*, "Passive synchronization of erbium and thulium doped fiber mode-locked lasers enhanced by common graphene saturable absorber," *Opt. Express*, vol. 22, no. 5, pp. 5536–5543, Mar. 2014.
[28] J. Xu *et al.*, "Graphene saturable absorber mirror for ultra-fast-pulse solid-state laser," *Opt. Lett.*, vol. 36, no. 10, pp. 1948–1950, May 2011.
[29] J. Ma *et al.*, "Graphene mode-locked femtosecond laser at 2 μm wavelength," *Opt. Lett.*, vol. 37, no. 11, pp. 2085–2087, Jun. 2012.
[30] L. Wei, D. Zhou, H. Fan, and W. Liu, "Graphene-based Q-switched erbium-doped fiber laser with wide pulse repetition rate range," *IEEE Photon. Technol. Lett.*, vol. 24, no. 4, pp. 309–311, Feb. 2012.
[31] B. V. Cunning, C. L. Brown, and D. Kielpinski, "Low-loss flake-graphene saturable absorber mirror for laser mode-locking at sub-200-fs pulse duration," *Appl. Phys. Lett.*, vol. 99, no. 26, Dec. 2011, Art. ID. 261109.
[32] Y. L. Chen *et al.*, "Experimental realization of a three-dimensional topological insulator, Bi_2Te_3," *Science*, vol. 325, no. 5937, pp. 178–181, Jun. 2009.
[33] S. S. Hong *et al.*, "Ultrathin topological insulator Bi_2Se_3 nanoribbons exfoliated by atomic force microscopy," *Nano Lett.*, vol. 10, no. 8, pp. 3118–3122, Jul. 2010.
[34] D. Teweldebrhan, V. Goyal, and A. A. Balandin, "Exfoliation and characterization of bismuth telluride atomic quintuples and quasi-two-dimensional crystals," *Nano Lett.*, vol. 10, no. 4, pp. 1209–1218, Mar. 2010.
[35] C. Wang *et al.*, "In situ Raman spectroscopy of topological insulator Bi_2Te_3 films with varying thickness," *Nano Res.*, vol. 6, no. 9, pp. 688–692, Sep. 2013.
[36] X. Li, B. Zhou, L. Pu, and J. Zhu, "Electrodeposition of Bi_2Te_3 and Bi_2Te_3 derived alloy nanotube arrays," *Cryst. Growth Des.*, vol. 8, no. 3, pp. 771–775, Feb. 2008.
[37] L. Ren *et al.*, "Large-scale production of ultrathin topological insulator bismuth telluride nanosheets by a hydrothermal intercalation and exfoliation route," *J. Mater. Chem.*, vol. 22, no. 11, pp. 4921–4926, Jan. 2012.
[38] E. E. Foos, R. M. Stroud, and A. D. Berry, "Synthesis and characterization of nanocrystalline bismuth telluride," *Nano Lett.*, vol. 1, no. 12, pp. 693–695, Oct. 2001.
[39] G. Zhang *et al.*, "Rational synthesis of ultrathin n-type Bi2Te3 nanowires with enhanced thermoelectric properties," *Nano Lett.*, vol. 12, no. 1, pp. 56–60, Nov. 2011.
[40] X. Zhao *et al.*, "Bismuth telluride nanotubes and the effects on the thermoelectric properties of nanotube-containing nanocomposites," *Appl. Phys. Lett.*, vol. 86, no. 6, Feb. 2005, Art. ID. 062111.
[41] Y. Chen *et al.*, "Large energy, wavelength widely tunable, topological insulator Q-switched erbium-doped fiber laser," *IEEE J. Sel. Top. Quantum Electron.*, vol. 20, no. 5, Sep. 2013, Art. ID. 0900508.
[42] S. M. J. Kelly, "Characteristic sideband instability of periodically amplified average soliton," *Electron. Lett.*, vol. 28, no. 8, pp. 806–807, Apr. 1992.
[43] C. Hönninger, R. Paschotta, F. Morier-Genoud, M. Moser, and U. Keller, "Q-switching stability limits of continuous-wave passive mode locking," *J. Opt. Soc. Amer. B*, vol. 16, no. 1, pp. 46–56, Jan. 1999.
[44] P. Černý, G. Valentine, D. Burns, and K. McEwan, "Passive stabilization of a passively mode-locked laser by nonlinear absorption in indium phosphide," *Opt. Lett.*, vol. 29, no. 12, pp. 1387–1389, Jun. 2004.
[45] Y. Chen *et al.*, "Self-assembled topological insulator-Bi_2Se_3 membrane as a passive Q-switcher in an erbium-doped fiber laser," *IEEE J. Lightw. Technol.*, vol. 31, no. 17, pp. 2857–2863, Jul. 2013.